

To be appeared in AJ

# Low- and Medium-Dispersion Spectropolarimetry of Nova V475 Sct (Nova Scuti 2003): Discovery of an Asymmetric High-Velocity Wind in a Moderately Fast Nova<sup>1</sup>

Koji S. Kawabata<sup>2</sup>, Youichi Ohyama<sup>3,4</sup>, Noboru Ebizuka<sup>5</sup>, Tadafumi Takata<sup>3,6</sup>, Michitoshi Yoshida<sup>7</sup>, Mizuki Isogai<sup>8</sup>, Yuji Norimoto<sup>7</sup>, Akira Okazaki<sup>9</sup>, and Masashi S. Saitou<sup>9</sup>

## ABSTRACT

We present low-resolution ( $R \sim 90$ ) and medium-resolution ( $R \sim 2500$ ) spectropolarimetry of Nova V475 Sct with the HBS instrument, mounted on the 0.91-m telescope at the Okayama Astrophysical Observatory, and with FOCAS, mounted on the 8.2-m Subaru telescope. We estimated the interstellar polarization toward the nova from the steady continuum polarization components and H $\alpha$  line emission components. After subtracting the interstellar polarization component from the observations, we found that the H $\alpha$  emission seen on 2003 October

---

<sup>1</sup>Based on data obtained at the Subaru Telescope and the Okayama Astrophysical Observatory, which are operated by the National Astronomical Observatory of Japan (NAOJ)

<sup>2</sup>Hiroshima Astrophysical Science Center, Hiroshima University, 1-3-1 Kagamiyama, Higashi-Hiroshima, Hiroshima 739-8526, Japan; kawabtkj@hiroshima-u.ac.jp.

<sup>3</sup>Subaru Telescope, NAOJ, 650 North A'ohoku Place, Hilo, HI 96720, USA; ohyama@naoj.org, takata@naoj.org.

<sup>4</sup>Department of Infrared Astrophysics, ISAS, Japan Aerospace Exploration Agency (JAXA), 3-1-1 Yoshinodai, Sagami-hara, Kanagawa 229-8510, Japan.

<sup>5</sup>Integrated V-CAD System Research Program, RIKEN (The Institute of Physical and Chemical Research), Wako, Saitama 351-0198, Japan; ebizuka@riken.jp.

<sup>6</sup>Astronomical Data Analysis Center, NAOJ, 2-21-1 Osawa, Mitaka, Tokyo 181-8588, Japan.

<sup>7</sup>Okayama Astrophysical Observatory, NAOJ, 3037-5 Honjo, Kamogata-cho, Asakuchi-gun, Okayama 719-0232, Japan; yoshida@oao.nao.ac.jp, agk00226@v1.yct.ne.jp

<sup>8</sup>Kiso Observatory, Institute of Astronomy, University of Tokyo, Mitake-mura, Kiso-gun, Nagano 397-0101, Japan; iso@kiso.ioa.s.u-tokyo.ac.jp.

<sup>9</sup>Department of Science Education, Gunma University, Aramaki 4-2, Maebashi 371-8510, Japan; okazaki@edu.gunma-u.ac.jp, saitou-m@ed.edu.gunma-u.ac.jp.

7 was clearly polarized. In the polarized flux spectrum, the H $\alpha$  emission had a distinct red wing extending to  $\sim +4900 \text{ km s}^{-1}$  and a shoulder around  $+3500 \text{ km s}^{-1}$ , showing a constant position angle of linear polarization  $\theta_* \simeq 155^\circ \pm 15^\circ$ . This suggests that the nova had an asymmetric outflow with a velocity of  $v_{\text{wind}} \simeq 3500 \text{ km s}^{-1}$  or more, which is six times higher than the expansion velocity of the ionized shell at the same epoch. Such a high-velocity component has not previously been reported for a nova in the ‘moderately fast’ speed class. Our observations suggest the occurrence of violent mass-loss activity in the nova binary system even during the common-envelope phase. The position angle of the polarization in the H $\alpha$  wing is in good agreement with that of the continuum polarization found on 2003 September 26 ( $p_* \simeq 0.4\text{--}0.6 \%$ ), which disappeared within the following 2 d. The uniformity of the PA between the continuum polarization and the wing polarization on October 7 suggests that the axis of the circumstellar asymmetry remained nearly constant during the period of our observations.

*Subject headings:* circumstellar matter — novae, cataclysmic variables — polarization — stars: individual (V475 Sct) — stars: winds, outflows

## 1. Introduction

It is generally accepted that the outburst of a classical nova is due to a thermonuclear runaway in a hydrogen-rich envelope accreted onto a white dwarf in a semi-detached binary system. The outburst ejects  $\sim 10^{-4} M_\odot$  of matter from the white dwarf surface with velocities up to several thousand  $\text{km s}^{-1}$  (see, e.g., Bode & Evans 1989). The study of nova outburst has consequences for a number of areas, including the study of nucleosynthesis in the accreted envelope, the processes of dust formation in the ejected matter, and the gas dynamics and chemical evolution of the interstellar medium.

The shapes of the outburst ejecta provide an insight into the physical processes that occur during outbursts. Deep imaging and spectroscopic observations of old nova remnants have revealed that many of them have asymmetric structures, such as prolate shells including rings and blobs (e.g., Slavin, O’Brien, & Dunlop 1995; Paresce et al. 1995; Gill & O’Brien 2000; Krautter et al. 2002; Harman & O’Brien 2003). In addition, polarimetry has revealed that the asymmetric geometry was already present at the outburst phase for many novae (Eggen, Mathewson, & Serkowski 1967; Zellner & Morrison 1971; Piirola & Korhonen 1979; Bergner et al. 1988; Kikuchi, Kondo, & Mikami 1988; Kučinskas 1990; Bjorkman et al. 1994; El’kin 1995; Okazaki et al. 1996; Johnson et al. 1997; Kawabata et al. 2001; Evans et al. 2002; Wisniewski et al. 2003; Desidera et al. 2004). However, despite the accumulation of

observational facts, it is still not clear what gives rise to departures from spherical symmetry in nova ejecta.

In a typical model of nova mass loss in the outburst phase, the ejecta are presumed to consist of an initially ejected main shell and a steadily blowing faster wind. In this model, the different expansion velocities of the shell and the wind should cause them to collide. Using such an interacting wind model, Lloyd, O’Brien, & Bode (1997) carried out hydrodynamic simulations of the ejecta and were able to explain some of the observed structures, such as polar blobs and equatorial bands. In their model, the secondary star experiences a frictional drag force inside the common envelope and transfers angular momentum to the ejecta (cf., MacDonald 1986; Livio et al. 1990), causing a fast anisotropic flow that collides with the outer spherical shell. However, the effects of a rapidly rotating white dwarf may also be important (Porter, O’Brien, & Bode 1998; Scott 2000). Centrifugal forces reduce the effective surface gravity of the white dwarf at the equator and the electron degeneracy at the base of the accreted envelope becomes stronger at the poles. The ejected material gains higher velocities in the polar regions than at the equator regions, which gives rise to a high-velocity bipolar outflow. More recently, a transient high-velocity emission component was found in Nova V1494 Aql during its transition phase (Iijima & Esenoglu 2003), and Retter (2004) suggested that a temporary increase in the accretion rate resulted in the formation of a jet at the inner boundary of a reformed accretion disk (cf., Soker & Lasota 2004).

These studies assume or predict that the nova wind is highly asymmetric. If free electrons inside high-velocity winds scatter substantial amounts of the NLTE line emission from lower-velocity regions near the central star, redshifted, polarized light can be expected to contribute to the net flux, which will result in a broad red wing associated with an emission line in the polarized flux spectrum. Thus, spectropolarimetry with substantial wavelength resolution has the potential to provide us with unique information on the structure and kinematics of nova winds.

Nova V475 Sct (= Nova Scuti 2003) was discovered by H. Nishimura on 2003 August 28.58 UT (Nakano et al. 2003) and reached its maximum brightness of  $V_{\text{max}} = 8.43$  on September 1.77 UT (JD = 2,452,884.27; Chochol et al. 2005, see also Stringfellow & Walter 2004 and Morgan et al. 2005). In this paper, we consider this time as 0 d of the nova epoch. Yamaoka, Monard, & Rodriguez (2003) reported that the precise position is  $\alpha_{2000} = 18^{\text{h}}49^{\text{m}}37^{\text{s}}.600$  and  $\delta_{2000} = -9^{\circ}33'50''.85$  ( $l = 24^{\circ}20'$ ,  $b = -3^{\circ}95'$ ) and that no object is found within  $2''$  on the red 1984 DSS image or 1999 2MASS public images. The  $V$ -band lightcurve showed small irregular variations in the early decline phase, followed by a deep decline at  $\sim 60 - 200$  d (Chochol et al. 2005). The early decline rate of V475 Sct was  $t_2 \simeq 48$  d

<sup>1</sup> (Chochol et al. 2005;  $t_n$  is the time required for the nova to diminish by  $n$  magnitudes below maximum light), which suggests that the speed class of V475 Sct is ‘moderately fast’ ( $t_2 = 26\text{--}80$  d; Payne-Gaposchkin 1957). An optical spectrum obtained around maximum brightness (Siviero, Marrese, & Munari 2003; Morgan et al. 2005) displayed many emission lines such as Fe II and Balmer series lines, characteristic of Fe II novae (Williams 1992). Chochol et al. (2005) noted the photometric and spectroscopic similarities to V705 Cas and suggested that V475 Sct is a dusty nova (Gehrz 1988; Mason et al. 1998). In this paper, we present the results of our spectropolarimetry of V475 Sct in its outburst phase and discuss a high-velocity component seen in the polarized spectrum.

## 2. Observations and Data Reduction

### 2.1. Low-dispersion spectropolarimetry

We took low-resolution spectropolarimetry measurements of V475 Sct with HBS (the acronym stands for ‘Henkou-Bunkou-Sokkou-Ki,’ which means ‘spectro-photo-polarimeter’ in Japanese; Kawabata et al. 1999) attached to the Cassegrain focus of the 0.91-m telescope at the Okayama Astrophysical Observatory of NAOJ on 2003 September 26, 28, and 29 UT (25, 27, and 28 d, respectively). HBS uses a rotatable superachromatic half-wave plate and a fixed quartz Wollaston prism (manufactured by Oyokoden Lab.). Each polarization measurement consisted of several sets of four 200-250-s exposures corresponding to the four position angles of the wave plate,  $0^\circ$ ,  $22.5^\circ$ ,  $45^\circ$  and  $67.5^\circ$ . At the focal plane, we put two slitlets of the same dimension ( $3''.4 \times 24''$ ). One was for the target star and the other was for a nearby sky region. Thus, we simultaneously obtained four spectra, ordinary and extraordinary rays of both the target and the sky, with a back-illuminated SITe CCD ( $512 \times 512$ ,  $24 \mu\text{m}/\text{pixel}$ ). This configuration resulted in a spectral resolution of  $\Delta\lambda \simeq 70 \text{ \AA}$  and  $R = \lambda/\Delta\lambda \simeq 90$ . A log of the observations is given in Table 1.

The data were reduced using the *HBSRED* package (Kawabata et al. 1999). Both the

---

<sup>1</sup>Morgan et al. (2005) derives  $t_2 = 22$  d from AAVSO light curve data, which is considerably shorter than that derived by Chochol et al. (2005). In this paper, we adopt the latter because the maximum brightness  $V_{\text{max}} = 8.0 \pm 0.2$  in Morgan et al. (2005) is based on the very short flare seen in the curve around September 1.8 UT and such a short variation would have been unlikely to be considered in classifications of earlier novae, and Morgan et al. (2005) took the dip seen in the lightcurve on 2003 September 23–30 ( $\Delta V \simeq 0.4 - 0.6$ ) into account in deriving  $t_2$ ; however, this dip seems likely to be a local oscillation rather than a general brightness variation, given the global tendency of the lightcurve. The oscillation and deep decline of the lightcurve are typically seen in a subclass of moderately fast novae (Payne-Gaposchkin 1957).

instrumental polarization and depolarization were derived from unpolarized standard star (UP; Wolff et al. 1996; Serkowski 1974) data obtained with and without inserting a Glan-Taylor prism. The zero point of the position angle was determined from the observations of strongly polarized standard stars (SP; Wolff et al. 1996; Schmidt, Elston, & Lupie 1992) in the synthesized  $V$  band. All the adopted calibration data were obtained during the 2003 July–September run with the same focal slitlets as used for the nova observations. The magnitude of the derived instrumental polarization was approximated by a smooth function of wavelength. To give some examples, its magnitude was  $0.363 \pm 0.002$  % at  $5000 \text{ \AA}$  and  $0.393 \pm 0.010$  % at  $8000 \text{ \AA}$  (the error is the mean error of a total 31 UP observations). This instrumental polarization was vectorially subtracted from the observational data. The polarimetric stability, estimated from the peak-to-peak variation of UP polarization in the observation period (a total of four observations for 107 Psc and  $\kappa$  Cet), was less than 0.1 % over the observed wavelength range. A correction was also made for the zero point of the position angle; its accuracy is estimated to be  $0^\circ.40$ , which is the  $1\sigma$  range for a total of 11 SP observations during the July–September run.

## 2.2. Medium-dispersion spectropolarimetry

Our other spectropolarimetric observations of V475 Sct were carried out with the Faint Object Camera And Spectrograph (FOCAS; Kashikawa et al. 2002), attached to the Cassegrain focus of the 8.2-m Subaru telescope (Kaifu et al. 2000; Iye et al. 2004) on 2003 October 7.29 UT (36 d). The polarimetric module consists of a rotating superachromatic half-wave plate and a fixed quartz Wollaston prism (manufactured by B. Halle Nachfl.), and both the ordinary and the extraordinary rays are simultaneously recorded on two MIT/LL CCDs ( $2k \times 4k$ ,  $15 \mu\text{m}/\text{pixel}$ ). We used a  $0''.4$  width  $\times$   $20''.6$  length slit and a  $665 \text{ lines mm}^{-1}$  volume-phase holographic (VPH) grism (Ebizuka et al. 2003), which gives a wavelength coverage of  $5300\text{--}7700 \text{ \AA}$  and a spectral resolution of  $\simeq 2.6 \text{ \AA}$  and  $R \simeq 2500$ . The corresponding reciprocal spectral dispersion was  $0.605 \text{ \AA}/\text{pixel}$ . To our knowledge, this is the highest resolution spectropolarimetry for a classical nova in the literature. To eliminate the contamination due to second-order spectra, a sharp-cut filter Y47 was used together with the VPH grism. The observation consisted of two sets of four sequential integrations at the  $0^\circ.0$ ,  $45^\circ.0$ ,  $22^\circ.5$  and  $67^\circ.5$  positions of the half-wave plate (Table 1).

The frames were reduced using the standard methods for CCD spectroscopy. Since no nearby object was seen in the images we obtained, we estimated the sky background component by a simple interpolation of the spectra at both sides of the object along the slit. The measurements of flatfield lamps through fully polarizing filters indicated that the

depolarization factor was negligible ( $\lesssim 0.05$ ) and we made no correction for it. The zero point of the position angle on the sky was determined from the SP observation (Schmidt, Elston, & Lupie 1992). The typical accuracy of the position angle is estimated to be  $0^\circ.16$ , which is the  $1\sigma$  value for a total of 13 observations of HD 204827 in 2002 June through 2003 June.

Higher-resolution spectropolarimetry ( $R \gtrsim 2000$ ) sometimes suffers from a strong spectral modulation in polarization (*ripple* pattern) due to multiple reflections within the wave plate (e.g., Aitken & Hough 2001; Ikeda et al. 2003; Clarke 2005). In that case some method must be applied, as part of the data reduction procedure, to remove the pattern (e.g., Harries & Howarth 1996). Figure 1 shows the polarization spectra obtained for the unpolarized star HD 212311 with the same optical configuration as the target observation. One can observe that the peak amplitude is less than 0.2 % in the instrumental  $Q$ ,  $U$  spectra and that the ripple pattern is not significant in our data. One possible reason for this is that the somewhat poorer surface accuracy of the wave plate, due to the four block construction for a large aperture (125 mm  $\phi$ ), effectively reduces the ripple effect (Aitken & Hough 2001). Therefore, we were able to analyze the data in a standard way, except for the application of a slight correction for the nearly wavelength-independent instrumental polarization ( $Q_{\text{instr}}$ ,  $U_{\text{instr}} \lesssim 0.1$  %; Figure 1). Many calibration observations during 2002–2003 suggest that the polarimetric stability and accuracy of Subaru/FOCAS are equal to or less than 0.05 % (Kawabata 2005).

### 3. Results and Discussion

#### 3.1. Spectroscopic evolution

Figure 2a shows the low-dispersion spectra of V475 Sct on 25, 27 and 28 d. We see many prominent emission lines, e.g., Balmer series, Na I D  $\lambda\lambda 5890, 5896$ , O I  $\lambda 7773$ , O I  $\lambda 8446$ , Ca II IR triplet and Fe II multiplets. At this epoch the [O I]  $\lambda\lambda 6300, 6364$  forbidden emission lines are still weak. In the medium-dispersion spectrum obtained on 36 d (Figure 3a), we can see resolved features of these lines at 5300–7700 Å. The Na I D doublet shows complicated features consisting of multiple P Cygni profiles, on which sharp interstellar absorption lines are superimposed at  $\sim +75$  km s $^{-1}$ . The permitted lines, H $\alpha$  and Fe II  $\lambda 6248$ , have P Cygni absorption components at  $-650$  and  $-1500$  km s $^{-1}$  (Figure 4). The former component is likely to correspond to the absorption features seen at  $-500$  km s $^{-1}$  on  $-1$  d (Boeche & Munari 2003),  $-480$  km s $^{-1}$  on 14 d, and  $-640$  km s $^{-1}$  on 24 d (Chochol et al. 2005). Thus, it appears that this component was accelerated principally at 14–24 d during the  $\sim 40$  post-maximum days. However, the latter, faster component seems to correspond to the feature that was seen at  $-1140$  km s $^{-1}$  on 14 d, and  $-1370$  km s $^{-1}$  on 24 d (Chochol et al. 2005),

which implies a monotonic acceleration for this component. The forbidden [O I]  $\lambda\lambda 6300, 6364$  lines are well developed by the epoch of our medium-dispersion observations. The profile of [O I]  $\lambda 6300$  has a flat top and steep edges at both sides, suggesting that the lines originate in the expanding shell (e.g., Gill & O’Brien 1999). The FWHM/2 of this emission line is  $\sim 550 \text{ km s}^{-1}$ , which is comparable with the blueshift of the P-Cyg absorption component seen in  $\text{H}\alpha$  and Fe II  $\lambda 6248$ . These are consistent with a picture in which V475 Sct at that epoch had a main shell expanding at a velocity of  $v_{\text{exp}} \simeq 600 \pm 50 \text{ km s}^{-1}$  and a nova wind with a speed  $\sim 2.5$  times faster than the shell along the line of sight.

We note that the  $\text{H}\alpha$  emission line has a considerably asymmetric profile, with a red wing extending beyond  $+2000 \text{ km s}^{-1}$ . We will discuss the origin of the broad red wing in §3.3.

### 3.2. Interstellar polarization

Aligned nonspherical dust grains in interstellar media produce interstellar polarization (ISP). In order to evaluate the component of polarization intrinsic to the nova, the ISP must be properly subtracted from the observed polarization. Taking into account that the position angle (PA) of the intrinsic polarization,  $\theta_*$ , and that of the ISP,  $\theta_{\text{isp}}$ , are independent of each other, and also the fact that  $\theta_{\text{isp}}$  is almost constant as a function of wavelength, the observed Stokes parameters ( $q_{\text{obs}}$ ,  $u_{\text{obs}}$ ) may be written as

$$\begin{aligned} q_{\text{obs}}(\lambda) &= p_*(\lambda) \cos 2\theta_*(\lambda) + p_{\text{isp}}(\lambda) \cos 2\theta_{\text{isp}} , \\ u_{\text{obs}}(\lambda) &= p_*(\lambda) \sin 2\theta_*(\lambda) + p_{\text{isp}}(\lambda) \sin 2\theta_{\text{isp}} , \end{aligned} \quad (1)$$

where  $\lambda$  is the wavelength, and  $p_*(\lambda)$  and  $p_{\text{isp}}(\lambda)$  are the magnitudes of polarization of the component intrinsic to the nova and the ISP component, respectively.  $p_{\text{isp}}(\lambda)$  is found to be well represented by an empirical function of wavelength:

$$p_{\text{isp}}(\lambda) = p_{\text{max}} \exp[-1.15 \ln^2(\lambda_{\text{max}}/\lambda)] , \quad (2)$$

where the maximum ISP,  $p_{\text{max}}$ , occurs at the wavelength  $\lambda_{\text{max}}$  (Serkowski, Mathewson, & Ford 1975).

Figures 2 and 3 demonstrate the observed polarization spectra. A distinct polarization displacement occurred between 25 d and 27 d; the magnitude of polarization decreased by 0.2–0.4 % and the PA rotated by  $10^\circ$ – $25^\circ$  in the continuum light at 4500–8500 Å. A clear depolarization effect across the  $\text{H}\alpha$  emission line was also seen on 25 d. NLTE line emission is generally formed in the outer ionized region and is subject to smaller Thomson scattering optical depth compared to the continuum light from the embedded central star. This leads to

a lower polarization of line emission than that of neighboring continuum light (Harrington & Collins 1968; Schulte-Ladbeck, Meade, & Hillier 1992). Therefore, the depolarization effect provides us with evidence that the continuum light on 25 d was intrinsically polarized. However, the continuum polarization remained almost constant from 27 d through 36 d. In this period the polarization spectra could be represented by a smooth curve, gradually decreasing with wavelength, and the PA was almost constant around  $110^\circ$ . There was no clear line polarization effect across the  $H\alpha$  line on 27 and 28 d. These results suggest that the steady continuum polarization component predominantly represents the ISP.

Here we adopt three methods to estimate the ISP toward V475 Sct. One is to derive the almost invariable continuum polarization on 27–36 d (method 1), the second is to average the observed polarization in the  $H\alpha$  line band on 25–28 d (method2), and the third is to subtract the continuum component from the result of method2 and to derive the polarization component of the pure  $H\alpha$  line emission (method 3).

For method 1, we obtained the following ISP parameters by a nonlinear regression of Equation (2) for the polarimetric data on 27–36 d:  $p_{\max} = 0.701 \pm 0.016 \%$ ,  $\lambda_{\max} = 4470 \pm 120 \text{ \AA}$  and  $\theta_{\text{isp}} = 111^\circ.9 \pm 0^\circ.3$ . In this calculation, we neglect the  $H\alpha$  line region (see method 2) because the possibility of contamination due to the intrinsic polarization component (as seen on 36 d) cannot be ruled out.

For method 2, we adopted the wavelength region from 6490 to 6660  $\text{\AA}$  as the  $H\alpha$  line band and vectorially averaged the observed polarization. In this method, although the derived polarization is still contaminated by the continuum component, we can neglect it because the emission line flux is much higher than the continuum flux (e.g., Taylor et al. 1991; Schulte-Ladbeck et al. 1993, 1994). The derived daily values at  $H\alpha$  on three nights are shown in the upper part of Table 2, along with their  $\sigma$ -weighted-mean values.

For method 3, we adopted the same wavelength region for  $H\alpha$  line band as in method 2. In subtracting the continuum component from the line band data, we used two wavelength regions on both sides of the line, each of 200  $\text{\AA}$  width, in which no significant polarization feature is seen. The derived line emission components are shown in the lower part of Table 2.

We obtained  $p_{\max} = 0.698 \pm 0.043 \%$  and  $p_{\max} = 0.695 \pm 0.056 \%$  using method 2 and 3, respectively, assuming that  $\lambda_{\max}$  takes the same value as that of method 1. The derived ISP parameters are summarized in Table 3. There is no significant difference between the results derived using the three different methods, and we will refer to the results of method 1 and 3 in the following discussion. (Method 2 gives values that are intermediate between those of methods 1 and 3.) The derived ISP components are plotted in Figures 2 and 3.



They show that both ISP curves well trace the continuum polarization on 27–36 d and also the  $H\alpha$  line polarization on 25–28 d. In Figure 2 the magnitude of polarization at a data point close to the  $H\alpha$  line core on 25 d is somewhat ( $1.1\sigma$ ) lower than the ISP curves, but we consider the difference at this bin to be insignificant because the width of the bin,  $\Delta\lambda = 22$  Å, is considerably narrower than the wavelength resolution (see also Table 2).

Figure 5 shows a map of the polarization of the field stars around V475 Sct (Heiles 2000). Since the distance toward V475 Sct has been estimated to be  $4.8 \pm 0.9$  kpc (Chochol et al. 2005), we selected field stars at 3–7 kpc. Generally we can use the field star technique only when we know the distance toward the target star with a substantial accuracy and also have either a field star containing no intrinsic polarization or plenty of field stars to cancel out their intrinsic components by averaging. In the present case, the error of the distance estimation for V475 Sct is somewhat large and we have only a few sample stars close to the target in 3D space. We thus use the map only for a rough check. The three closest stars (HD 173987, HD 170716, and HD 173694) are unlikely to have substantial intrinsic polarization because they do not have emission lines (although they are all supergiants and may exhibit small variability). Although V475 Sct shows an unusually small ratio  $p_{\max}(\%)/E_{B-V} \simeq 1.0$  compared with typical values for the Galactic interstellar medium ( $p_{\max}/E_{B-V} \simeq 2-9$ ; Figure 9 of Serkowski, Mathewson, & Ford 1975), its ratio is nearly consistent with those of the nearest three stars,  $p/E_{B-V} \simeq 1.3-1.4$ . This is likely to be because random components are predominant for the Galactic magnetic fields projected to the plane of sky in this direction,  $l \sim 24^\circ$  (related with the direction of the Cygnus-Orion spiral arm; Fosalba et al. 2002) and the polarizing efficiency against the color excess is remarkably low. However, when we choose two stars (HD 173987 and HD 173694) from the viewpoint of proximity in both angular and radial distances, the ISP component of V475 Sct seems roughly consistent with the ISP pattern inferred from those of the two stars. We therefore adopted the derived ISP parameters, and calculated the polarization component intrinsic to the nova using Equation (1).

### 3.3. The red wing of $H\alpha$ emission in the polarized spectrum

In Figure 6, we plot the intrinsic polarization around the  $H\alpha$  line on 25 and 36 d. There is no significant difference between the results of methods 1–3 for estimating the ISP. In the polarization data at 25 d we can see a ‘pure’ depolarization effect across the  $H\alpha$  emission line, in which the PA is almost constant against wavelength. The small polarization of the  $H\alpha$  line emission on 25 d ( $p_* \simeq 0.10-0.15$  %) should still be affected by the intrinsic continuum polarization.

In contrast, the polarization spectrum taken on 36 d indicates that the  $H\alpha$  line emission is clearly polarized both at the line core and the wing component, although the continuum light is not strongly polarized. Two distinct properties of the emission line can be seen in Figure 6: (1) The polarized flux ( $p_* \times$  total flux) on 36 d has a broad red wing component, which corresponds to the broad bump around 6640 Å in the  $p_*$  spectrum, and (2) the PA of the wing polarization is well aligned, with  $\theta_* \simeq 155^\circ \pm 15^\circ$ , from the center wavelength of  $H\alpha$  through the red edge of the wing  $\sim 6670$  Å. Since all the other lines, including Na I D and [O I], were too weak to be measured polarimetrically, we mainly discuss the  $H\alpha$  line polarization in what follows.

Is the red wing component really associated with the  $H\alpha$  emission? No other strong emission line near 6640 Å is known for typical novae at similar epochs, so that the red wing component could not be superimposed by another emission line. In addition, the PA of the intrinsic polarization is almost constant throughout the broad bump feature, including the  $H\alpha$  line core. We therefore consider that the wing component is in fact associated with the  $H\alpha$  line emission.

This polarized red wing component is naturally explained if a high-velocity collimated outflow is present near the  $H\alpha$  line emitting region at  $PA \simeq 65^\circ$  and/or  $245^\circ$  on the projected sky. If free electrons in a receding wind scatter a substantial amount of light emitted from the inner (i.e., lower velocity) region, the observed polarized flux will have a redshifted component, owing to contributions from both scattered and unscattered (i.e., direct) light from the inner region (see Figure 7). The flux scattered by a single wind is redshifted by

$$\Delta v_{\text{wind}} = (1 + \cos i) v_{\text{wind}} , \quad (3)$$

where  $v_{\text{wind}}$  is the velocity of the wind and  $i$  is the inclination angle of the wind direction against the line of sight measured from the far side of the nova. It should be noted that the flux scattered by a receding wind is always shifted redward  $\Delta v_{\text{wind}} \geq 0$  and that little or no polarization is expected for  $i \simeq 0^\circ$  or  $180^\circ$ , as the scattering angle is nearly zero. In a realistic case, any wind is more likely to be bipolar rather than to have a single direction of outflow. If we assume a bipolar wind, a double-peaked profile (with separation =  $2v_{\text{wind}} \cos i$ ) is expected in the polarization spectrum. In Figure 6b we find only a single broad peak around 6640 Å (corresponding to  $\Delta v_{\text{wind}} \simeq +3500$  km s<sup>-1</sup>) that extends up to 6670 Å (+4900 km s<sup>-1</sup>) from the constancy of  $\theta_*$ . This is consistent with a model in which the bipolar axis is approximately perpendicular to the line of sight (i.e.,  $i \sim 90^\circ$ ). In this case  $v_{\text{wind}}$  would be approximately equal to  $\Delta v_{\text{wind}}$  from Equation (3). Alternatively, the single peak can be explained for any  $i$  if we assume that one of the two scattered light components suffers from selective extinction (e.g., more absorption is expected for light scattered by the far-side wind component). In this case  $\Delta v_{\text{wind}}$  would indicate a lower limit on the real wind velocity,  $v_{\text{wind}}$ .

We conclude that the  $H\alpha$  wing polarization is more likely produced by scattering by a bipolar nova wind with a velocity of  $v_{\text{wind}} \simeq +3500 \text{ km s}^{-1}$  or higher. To our knowledge, such a high-velocity outflow has never been observed in moderately fast novae. This fact does not directly indicate that V475 Sct belongs to a peculiar category of novae. Rather, it is plausible that many past observations lacked the ability to detect such high-velocity outflows because of lower spectral resolution, insufficient time coverage, and/or lack of measurements of polarization properties.

### 3.4. Persistence of circumstellar asymmetric geometry

Figure 6 indicates the existence of significant continuum polarization (0.4–0.6 %) on 25 d. One can see that this continuum polarization extends over 4500–8400 Å with a similar magnitude and PA of polarization, although Figure 6 shows only a wavelength region near  $H\alpha$ . The intrinsic continuum polarization indicates that the asymmetric geometry was clearly present on 25 d. However, the polarization disappeared within the next 2 d. Thus, the continuum polarization component was not persistent but temporary, requiring a time-variable asymmetrical circumstellar geometry. We propose a plasma blob ejection as the most likely source of the temporary polarization. Assuming that the plasma blob ejection occurred just before 25 d, the blob would still be near the pseudo-photosphere and would not be outside of the expanding ionized shell. Such a blob would contribute effectively to the polarization of the continuum light from the pseudo-photosphere.

The similarity of the measured PA for the continuum polarization on 25 d and the wing polarization on 36 d suggests a persistence of the asymmetric geometry during this period. This scenario seems consistent with the polarimetric variability found in Novae V1974 Cyg and V1494 Aql in outburst phase; in these systems, the principal geometry of the nova wind remained nearly constant throughout the early decline phase, while clumpy mass ejection became conspicuous in the later phase (Bjorkman et al. 1994; Kawabata et al. 2001). It remains unclear whether the plasma blob causing the continuum polarization on 25 d also had a high velocity. Future high-spatial-resolution imaging of the remnant of V475 Sct may give clues to the validity of this scenario.

### 3.5. Asymmetric high velocity wind

Our observations suggest that a violent mass-loss mechanism may exist even in a moderately fast nova. Evidence of high-velocity outflows ( $\gtrsim 2500 \text{ km s}^{-1}$ ) has been reported for

some recurrent novae, U Sco, CI Aql, and RS Oph (Iijima 2002; Anupama & Dewangan 2000; Kiss et al. 2001; Lépine et al. 1999; Taylor et al. 1989), and also for ONeMg classical novae, V838 Her, V1974 Cyg, V382 Vel and V1187 Sco (Ingram et al. 1992; Shore et al. 1993, 2003; Cassatella et al. 2004; Lynch et al. 2006). Those observations have shown that the peak expansion velocity is usually recorded near maximum light and that the velocity decreases as the optical light fades. It is likely that in these systems the outer shell is considerably accelerated directly after the initial ejection. This situation seems clearly different from that of typical classical novae, in which the expansion velocity gradually increases after maximum light, and later spectral systems of novae generally show higher expansion velocities (McLaughlin 1960; Bode & Evans 1989). It would therefore be better to discuss the wind of V475 Sct separately from the high-velocity outflows found in recurrent novae and ONeMg novae (cf. Friedjung & Duerbeck 1993).

Among normal classical novae (= CNO novae), only novae belonging to the ‘very fast’ speed class ( $t_2 < 10$  d) have shown high-velocity winds, e.g.,  $4000 \pm 50$  km s<sup>-1</sup> in V1500 Cyg ( $t_2 \sim 2$  d; Duerbeck & Wolf 1977). It is empirically known that the expansion velocity of a classical nova becomes higher as  $t_2$  is shorter, which has been explained in terms of the equipartition of energy between the radiation field and the ejected matter (Shara 1981). Optically thick wind calculations have shown that the nova lightcurve and maximum wind velocity depend primarily on the white dwarf mass,  $M_{\text{WD}}$ , and are less sensitive to the abundance (e.g., Kato & Hachisu 1994; Kato 1997, 1999), in the sense that a more massive white dwarf usually shows a more rapid decline in a nova outburst. However, even for the cases with the most massive white dwarfs, spherically symmetric models cannot well reproduce photospheric velocities of more than  $\sim 2000$  km s<sup>-1</sup>. Calculations of nova evolutionary sequences have also given similar results (Prialnik & Kovetz 1995).

As mentioned in §1, however, evidence for nonspherical ejecta have been found in many novae. Kato & Hachisu (2003) applied an asymmetric jet-shaped outflow in their steady-state mass-loss model and successfully reproduced the high-velocity outflows with speeds up to  $\sim 5000$  km s<sup>-1</sup> found in U Sco near maximum light. They suggested that the terminal velocity of the outflow is sensitive only to the white dwarf mass, as in the spherically symmetric models, and that neither the composition nor the opening angle of the jetlike outflow has a strong effect on the velocity. The white dwarf mass of U Sco is estimated to be  $M_{\text{WD}} \sim 1.37 M_{\odot}$  (Hachisu et al. 2000), which is higher than those of moderately fast or slower class novae ( $M_{\text{WD}} \lesssim 1.0 M_{\odot}$ , Livio 1992; Prialnik & Kovetz 1995). For  $M_{\text{WD}} \lesssim 1.0 M_{\odot}$  cases, the maximum photospheric velocity is at most 1000–1500 km s<sup>-1</sup> in the steady jetlike wind model (Kato & Hachisu 2003). For V475 Sct, Chochol et al. (2005) derived  $M_{\text{WD}} = 0.73 \pm 0.07 M_{\odot}$  using their photometric data along with the formula given by Livio (1992). The existence of a steady high-velocity wind of  $\sim 3500$  km s<sup>-1</sup> is still unusual for a moderately fast nova

without any additional acceleration source.

We now briefly consider the possibility of a non-static activity in a nova system within the framework of astronomical jets. High-velocity asymmetric outflows are found in various astronomical objects, such as T Tauri stars, X-ray binaries, and active galactic nuclei. Livio (2000) reviewed past studies on jets and discussed the possibility that all types of objects accompanied with jets possess accretion disks. It has been known that some mass-accreting white dwarf systems, such as supersoft X-ray sources and symbiotic stars, exhibit evidence of jets (e.g., Sokoloski et al. 2004). However, no convincing evidence of jets has been found so far for classical and dwarf novae, although the configuration of the binary system is similar to those of supersoft X-ray sources and symbiotic stars. Soker & Lasota (2004) applied their jet-launching thermal model with an accretion disk to the cataclysmic binaries and suggested that a mass-accretion rate  $\dot{M}_{\text{WD}} \gtrsim 10^{-6} \text{ M}_{\odot} \text{ yr}^{-1}$  is required for the formation of a shock and subsequent mass ejection. Their result explains why jets have not been observed in classical and dwarf novae ( $\dot{M}_{\text{WD}} \lesssim 10^{-8} \text{ M}_{\odot} \text{ yr}^{-1}$ ). However, Iijima & Esenoglu (2003) recently found a transient high velocity component ( $-2900$  and  $+2830 \text{ km s}^{-1}$ ) in the transition phase of a very fast nova V1494 Aql 104 d after the light maximum. Retter (2004) discussed this component together with the X-ray activity found in the nova (e.g., Orio, Convington, & Ögelman 2001; Drake et al. 2003), and suggested that the existence of jets is expected for classical novae, owing to a possible temporary increase of the mass-accretion rate up to  $\dot{M}_{\text{WD}} \sim 10^{-6} \text{ M}_{\odot} \text{ yr}^{-1}$ . This scenario requires the existence of an accretion disk around the white dwarf. Although it is not well-known when the accretion disk is reestablished after its probable destruction during the nova outburst, some indirect evidence for the presence of accretion disks has been found for some novae a few months or years after the outburst (Leibowitz et al. 1992; Retter, Leibowitz, & Ofek 1997; Retter, Leibowitz, & Kovo-Kariti 1998). However, for a moderately fast nova ( $M_{\text{WD}} \lesssim 1.0 \text{ M}_{\odot}$ ) both the white dwarf and the secondary (assuming a typical binary separation of  $\sim 10^{11} \text{ cm}$ ) seem to be still deeply engulfed by the photosphere  $\sim 40 \text{ d}$  after the outburst (Figure 12 of Kato & Hachisu 1994). It is not likely that the accretion of mass from the secondary has resumed by 36 d in the case of V475 Sct.

Therefore, at the present time, we do not have any plausible explanation for the ejection of the inferred high-velocity component. In order to establish a realistic model, we need further spectropolarimetric observations and need to establish how the continuum and line polarization components evolve during the outburst phase of novae. Simultaneous radio or X-ray monitoring would be useful to find evidence for high-energy events around the central star, which might give rise to high-velocity ejecta.

#### 4. Conclusion

We have presented low- and medium-dispersion spectropolarimetry of a classical nova V475 Sct at four epochs in its early decline phase. We estimated the ISP component and subtracted it from the observed polarization. Our main results can be summarized as follows:

1. The low-dispersion spectropolarimetry revealed that the continuum light over most of the observed wavelength range was intrinsically polarized by  $\simeq 0.4 - 0.6$  % on 2003 September 26 UT (25 d). This polarization component almost disappeared in the next 2 d, requiring a time-variable asymmetric circumstellar geometry.
2. The medium-dispersion spectropolarimetry on October 7 UT (36 d) detected an intrinsic polarization component across the  $H\alpha$  emission line. This suggests the existence of a wind with speeds of  $v_{\text{wind}} \simeq 3500 \text{ km s}^{-1}$  or higher. Such a fast wind has never been reported in moderately fast novae. It is hard to explain how the wind was formed within the current framework of nova winds or jets.
3. The PAs of the above two polarization components were similar to each other,  $\theta_* \simeq 150\text{--}155^\circ$ . This suggests that the matter giving rise to scattering in the two cases may have been ejected in a similar asymmetric geometry.

Our results demonstrate the great utility of high-dispersion spectropolarimetry for the study of nova outflows. Further observations, however, are required.

We are grateful to staff members at Okayama Astrophysical Observatory for their kind support. We also thank members of the FOCAS team and staff members at Subaru telescope for the opportunity of the observation. Data reduction/analysis was in part carried out on the “sb” computer system operated by the Astronomical Data Analysis Center (ADAC) and Subaru telescope of NAOJ. This work was supported by a Grant-in-Aid from the Ministry of Education, Culture, Sports, Science and Technology of Japan (No. 17684004).

#### REFERENCES

- Aitken, D. K., & Hough, J. H. 2001, *PASP*, 113, 1300
- Anupama, G. C., & Dewangan, G. C. 2000, *AJ*, 119, 1359
- Bergner, Yu. K., Miroshnichenko, A. S., Yudin, R. V., Yutanov, N. Yu., Dzakusheva, K. G., Ilyin, V. V., Kuratov, K. S., & Mukanov, D. B. 1988, *Ap&SS*, 149, 63

- Boeche, C., & Munari, U. 2003, IAU Circ., 8191
- Bode, M. F., & Evans, A. 1989, *Classical Novae* (New York: John Wiley & Sons)
- Bjorkman, K. S., Johansen, K. A., Nordsieck, K. H., Gallagher, J. S., & Barger, A. J. 1994, *ApJ*, 425, 247
- Cassatella, A., Lamers, H. J. G. L. M., Rossi, C., Altamore, A., & González-Riestra, R. 2004, *A&A*, 420, 571
- Chochol, D., et al. 2005, *Contrib. Astron. Obs. Skalnaté Pleso*, 35, 107
- Clarke, D. 2005, *A&A*, 434, 377
- Desidera, S., et al. 2004, *A&A*, 414, 591
- Drake, J. J., et al. 2003, *ApJ*, 584, 448
- Duerbeck, H. W., & Wolf, B. 1977, *A&A Suppl.*, 29, 297
- Ebizuka, N., et al. 2003, *Proc. SPIE*, 4842, 319
- Eggen, O. J., Mathewson, D. S., & Serkowski, K. 1967, *Nature*, 213, 1216
- El’kin, V. G. 1995, *PAZh*, 21, 750
- Evans, A., Yudin, R. V., Naylor, T., Ringwald, F. A., & Koch Miramond, L. 2002, *A&A*, 384, 504
- Fosalba, P., Lazarian, A., Prunet, S., & Tauber, J. A. 2002, *ApJ*, 564, 762
- Friedjung, M., & Duerbeck, H. W. 1993, in *Cataclysmic Variables and Related Objects*, eds. M. Hack & C. la Dous (Washington, DC: NASA), 371
- Gehrz, R. D. 1988, *ARA&A*, 26, 377
- Gill, C. D., & O’Brien, T. J. 1999, *MNRAS*, 307, 677
- Gill, C. D., & O’Brien, T. J. 2000, *MNRAS*, 314, 175
- Hachisu, I., Kato, M., Kato, T., Matsumoto, K. 2000, *ApJ*, 528, L97
- Harman, D. J., & O’Brien, T. J. 2003, *MNRAS*, 344, 1219
- Harries, T. J., & Howarth, I. D. 1996, *A&A*, 310, 533

- Harrington, J. P., & Collins, G. W., II 1968, *ApJ*, 151, 1051
- Heiles, C. 2000, *AJ*, 119, 923
- Iijima, T. 2002, *A&A*, 387, 1013
- Iijima, T., & Esenoglu, H. H. 2003, *A&A*, 404, 997
- Ingram, D., Garnavich, P., Green, P., & Szkody, P. 1992, *PASP*, 104, 402
- Ikeda, Y., Akitaya, H., Matsuda, K., Kawabata, K. S., Seki, M., Hirata, R., & Okazaki, A. 2003, *Proc. SPIE*, 4843, 437
- Iye, M., et al. 2004, *PASJ*, 56, 381
- Johnson, J. J., et al. 1997, *AJ*, 113, 2200
- Kaifu, N., et al. 2000, *PASJ*, 52, 1
- Kashikawa, N., et al. 2002, *PASJ*, 54, 819
- Kato, M. 1997, *ApJS*, 113, 121
- Kato, M. 1999, *PASJ*, 51, 525
- Kato, M., & Hachisu, I. 1994, *ApJ*, 437, 802
- Kato, M., & Hachisu, I. 2003, *ApJ*, 587, L39
- Kawabata, K. S., et al. 1999, *PASP*, 111, 898
- Kawabata, K. S., et al. 2001, *ApJ*, 552, 782
- Kawabata, K. S. 2005, in *ASP Conf. Ser. 343, Astronomical Polarimetry: Current Status and Future Directions*, eds. A. Adamson, C. Aspin, & C. J. Davis (San Francisco: ASP), 238
- Kikuchi, S., Kondo, M., & Mikami, Y. 1988, *PASJ*, 40, 491
- Kiss, L. L., Thomson, J. R., Ogloza, W., Furész, G., & Sziládi, K. 2001, *A&A*, 366, 858
- Krautter, J., et al. 2002, *AJ*, 124, 2888
- Kučinskas, A. 1990, *Astron. Nachr.*, 311, 69



- Leibowitz, E. M., Mendelson, H., Mashal, E., Prialnik, D., & Seitter, W. C. 1992, *ApJ*, 385, L49
- Lépine, S., Shara, M. M., Livio, M., & Zurek, D. 1999, *ApJ*, 522, L121
- Livio, M. 1992, *ApJ*, 393, 516
- Livio, M. 2000, in *AIP Conf. Proc.* 522, *Cosmic Explosions*, eds. S. S. Holt & W. W. Zhang (Melville: AIP), 275
- Livio, M., Shankar, A., Burkert, A., & Truran, J. W. 1990, *ApJ*, 356, 250
- Lloyd, H. M., O’Brien, T. J., & Bode, M. F. 1997, *MNRAS*, 284, 137
- Lynch, D. K., et al. 2006, *ApJ*, 638, 987
- MacDonald, J. 1986, *ApJ*, 305, 251
- Mason, C. G., Gehrz, R. D., Woodward, C. E., Smilowitz, J. B., Hayward, T. L., & Houck, J. R. 1998, *ApJ*, 494, 783
- McLaughlin, D. B. 1960, in *Stellar Atmospheres*, ed. J. L. Greenstein (Chicago: Univ. Chicago Press).
- Morgan, G. E., Ringwald, F. A., Buil, C., & Garrett, M. 2005, *PASP*, 117, 938
- Munari, U., et al. 1999, *A&A*, 347, L39
- Nakano, S., Sato, H., Nishimura, H., Nakamura, T., Wakuda, S., Yamaoka, H., & Pearce, A. 2003, *IAU Circ.*, 8190
- Okazaki, A., et al. 1996, in *ASP Conf. Ser.* 97, *Polarimetry of the Interstellar Medium*, eds. W. G. Roberge & D. C. B. Whittet (San Francisco: ASP), 178
- Orio, M., Convington, J., & Ögelman, H. 2001, *A&A*, 373, 542
- Paresce, F., Livio, M., Hack, W., & Korista, K. 1995, *A&A*, 299, 823
- Payne-Gaposchkin, C. 1957, *The Galactic Novae* (Amsterdam: North-Holland)
- Pirola, V., & Korhonen, T. 1979, *A&A*, 79, 254
- Porter, J. M., O’Brien, T. J., & Bode, M. F. 1998, *MNRAS*, 296, 943
- Prialnik, D., & Kovetz, A. 1995, *ApJ*, 445, 789

- Retter, A., Leibowitz, E. M., & Ofek, E. O. 1997, MNRAS, 286, 745
- Retter, A., Leibowitz, E. M., & Kovo-Kariti, O. 1998, MNRAS, 293, 145
- Retter, A. 2004, ApJ, 615, L125
- Schmidt, G. D., Elston, R., & Lupie, O. L. 1992, AJ, 104, 1563
- Schulte-Ladbeck, R. E., Meade, M. R., & Hillier, D. J. 1992, in ASP Conf. Ser. 22, Non-isotropic and Variable Outflows from Stars, eds. L. Drissen, C. Leitherer, & A. Nota (San Francisco: ASP), 118
- Schulte-Ladbeck, R. E., Leitherer, C., Clayton, G. C., Robert, C., Meade, M. R., Drissen, L., Nota, A., & Schmutz, W. 1993, ApJ, 407, 723
- Schulte-Ladbeck, R. E., Clayton, G. C., Hillier, D. J., Harries, T. J., & Howarth, I. D. 1994, ApJ, 429, 846
- Scott, A. D. 2000, MNRAS, 313, 775
- Serkowski, K. 1974, in Planets, Stars and Nebulae studied with photopolarimetry, ed. T. Gehrels (Tucson: The University of Arizona Press), 135
- Serkowski, K., Mathewson, D. S., & Ford, V. L. 1975, ApJ, 196, 261
- Shara, M. 1981, ApJ, 243, 926
- Shore, S. N., Sonneborn, G., Starrfield, S., Gonzalez-Riestra, R., & Ake, T. B. 1993, AJ, 106, 2408
- Shore, S. N., et al. 2003, AJ, 125, 1507
- Siviero, S., Marrese, P. M., & Munari U. 2003, IAU Circ., 8199
- Slavin, A. J., O’Brien, T. J., and Dunlop, J. S. 1995, MNRAS, 276, 353
- Soker, N. & Lasota, J.-P. 2004, A&A, 422, 1039
- Sokoloski, J. L., Kenyon, S. J., Brocksopp, C., Kaiser, C. R., & Kellogg, E. M. 2004, Rev. Mexicana Astron. Astrofis., 20, 35
- Stringfellow, G. S., & Walter, F. M. 2004, AAS meeting 204, #63.04
- Taylor, A. R., Davis, R. J., Porcas, R. W., & Bode, M. F. 1989, MNRAS, 237, 81

- Taylor, M., Nordsieck, K. H., Schulte-Ladbeck, R. E., & Bjorkman, K. S. 1991, *AJ*, 102, 1197
- Porcas, R. W., & Bode, M. F. 1989, *MNRAS*, 237, 81
- Williams, R. E. 1992, *AJ*, 104, 725
- Wisniewski, J. P., Morrison, N. D., Bjorkman, K. S., Miroshnichenko, A. S., Gault, A. C., Hoffman, J. L., Meade, M. R., & Nett, J. M. 2003, *ApJ*, 588, 486
- Wolff, M. W., Nordsieck, K. H., & Nook, M. A. 1996, *AJ*, 111, 856
- Yamaoka, H., Monard, B., & Rodriguez, D. 2003, *IAU Circ.*, 8199
- Zellner, B., & Morrison, N. D. 1971, *AJ*, 76, 645

Table 1. Log of the observations

UT (epoch) 2003	JD 2,450,000+	Telescope/ Instrument	Wavelength (Å)	Res. $\lambda/\Delta\lambda$	Exposure <sup>a</sup> (sec)
Sep 26.53 (25 d)	2909.03	OA0 0.91m/HBS	4000–9000	90	200×24
Sep 28.49 (27 d)	2910.99	OA0 0.91m/HBS	4000–9000	90	250×24
Sep 29.48 (28 d)	2911.98	OA0 0.91m/HBS	4000–9000	90	250×24
Oct 07.29 (36 d)	2919.79	Subaru/FOCAS	5300–7700	2500	18×4+9×4

<sup>a</sup>The total exposure time is expressed as the integrated time per single frame, multiplied by the number of frames.

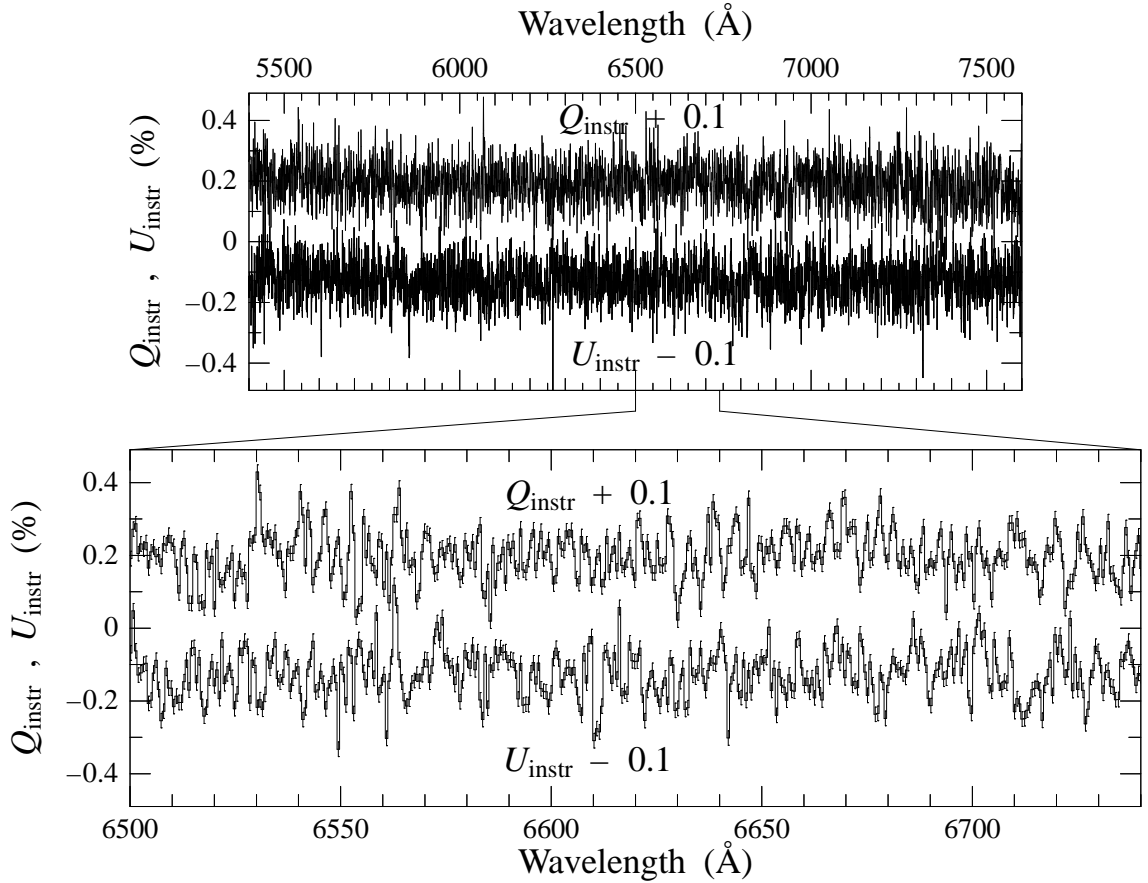


Fig. 1.— Instrumental polarization of Subaru/FOCAS. The data were obtained for an unpolarized standard star HD 212311, under the same optical configuration as used for the nova. In the observed polarization spectrum we do not see any significant ( $> 0.2\%$ ) ripple pattern, which has been a problem for some intermediate-dispersion spectropolarimetric observations.

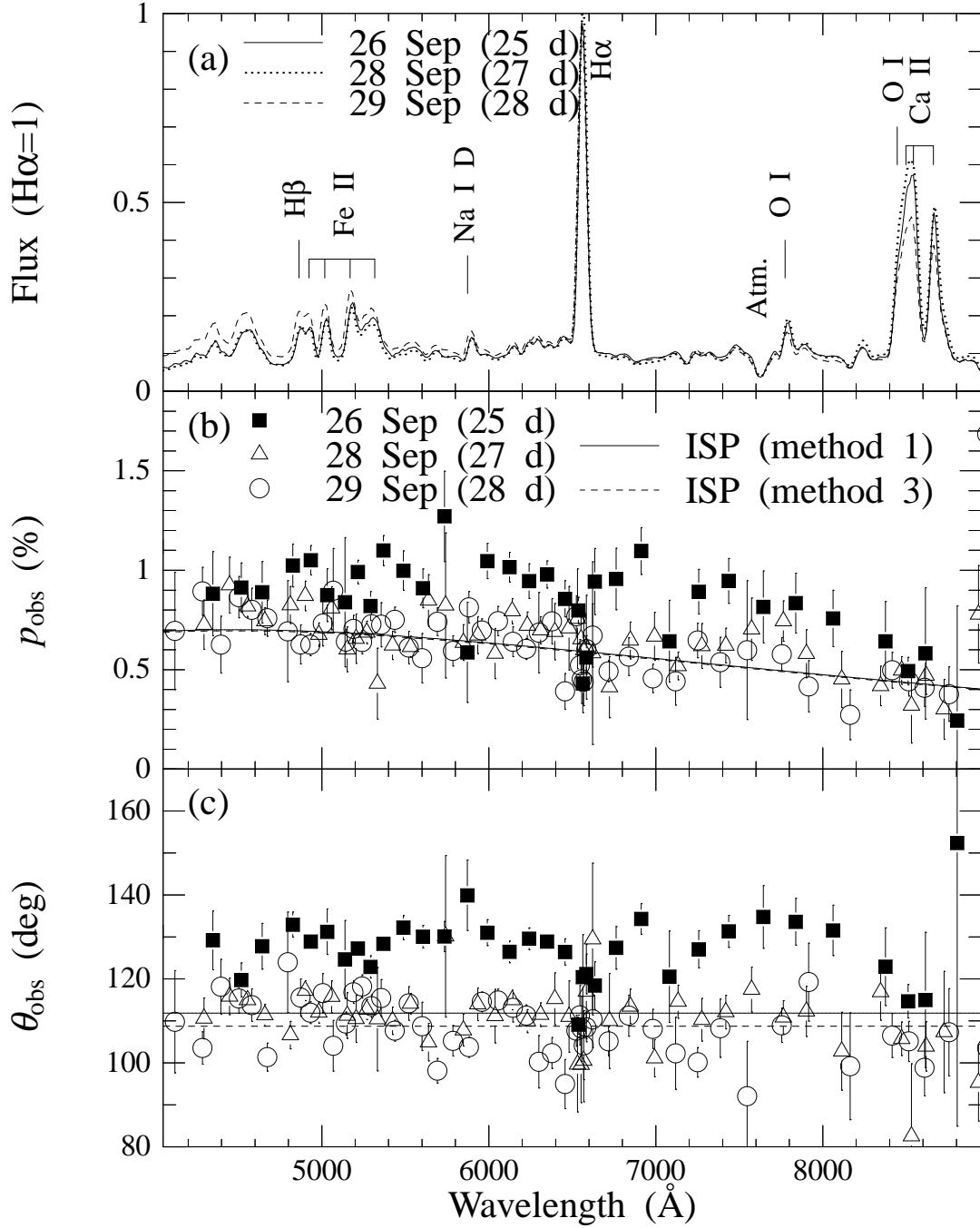


Fig. 2.— Spectropolarimetry of V475 Sct with HBS ( $\Delta\lambda = 70$  Å) on 2003 September 26–29 UT (25–28 d). From top to bottom we plot (a) the unbinned total flux, (b) the magnitude of the observed polarization, and (c) the position angle. Atmospheric extinction has not been corrected for, but the instrumental response has been calibrated. The major emission lines are identified by tick marks in (a). The polarimetric data are binned to a constant photon noise of 0.04 %, and the observational error ( $1\sigma$  variation among  $(Q, U)$  derived for each set of four exposures) in each bin is shown. The smooth solid and dashed lines in (b) and (c) panels are the ISP components, estimated as described in the text.

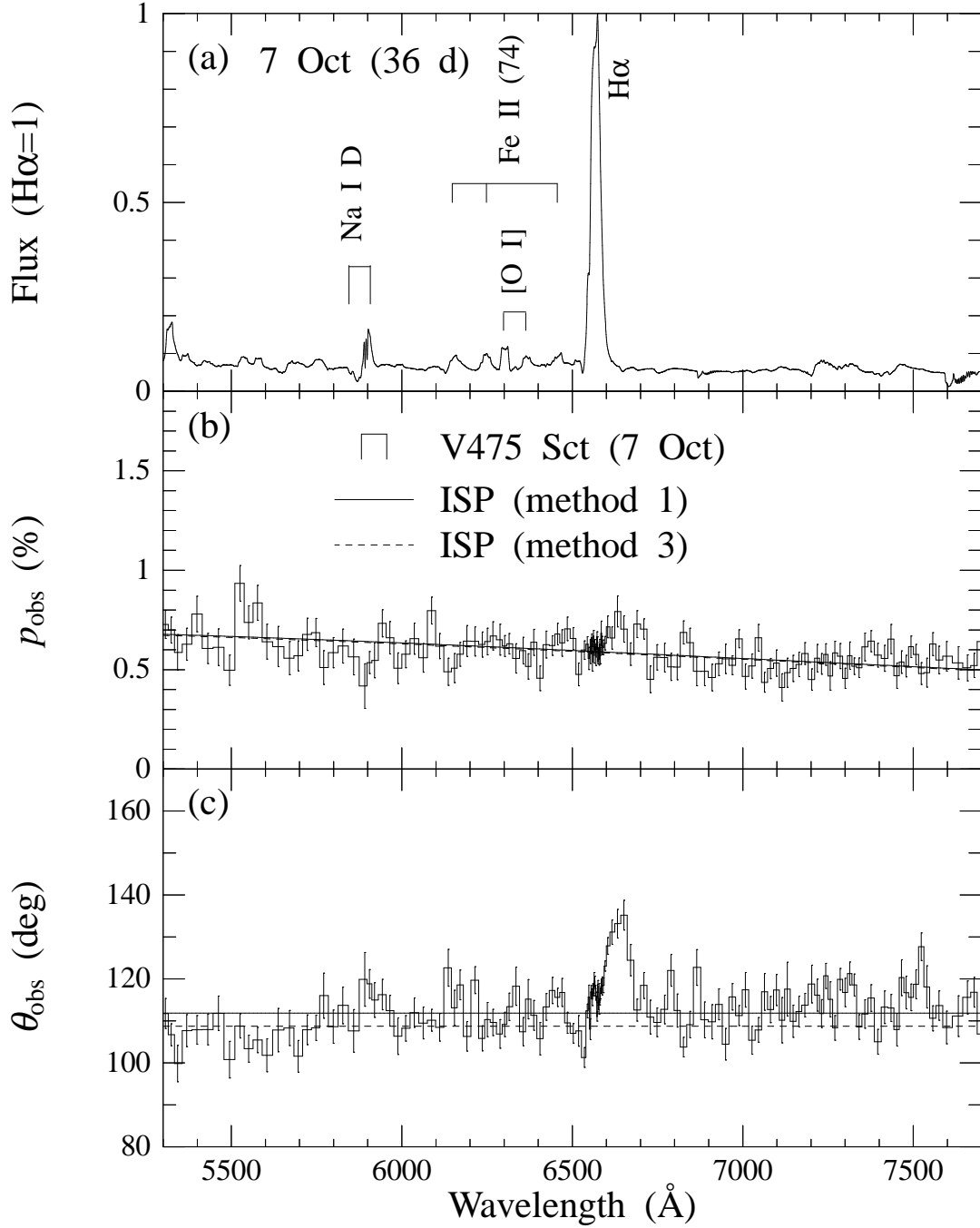


Fig. 3.— Spectropolarimetry of V475 Sct with FOCAS ( $\Delta\lambda = 2.6 \text{ \AA}$ ) on 2003 October 7 UT (36 d). The data are plotted in the same manner as in Figure 2, except that atmospheric extinction has been corrected for in (a). The error bar denotes the observational error ( $1\sigma$  variation of  $Q$  and  $U$  from pixel to pixel in each bin). The bump of  $\theta_{\text{obs}}$  around 6640  $\text{\AA}$  suggests the existence of a distinct polarization component, while the small dip at 6530  $\text{\AA}$  as well as the fluctuation around 6800  $\text{\AA}$  are likely to be noise-related artifacts.

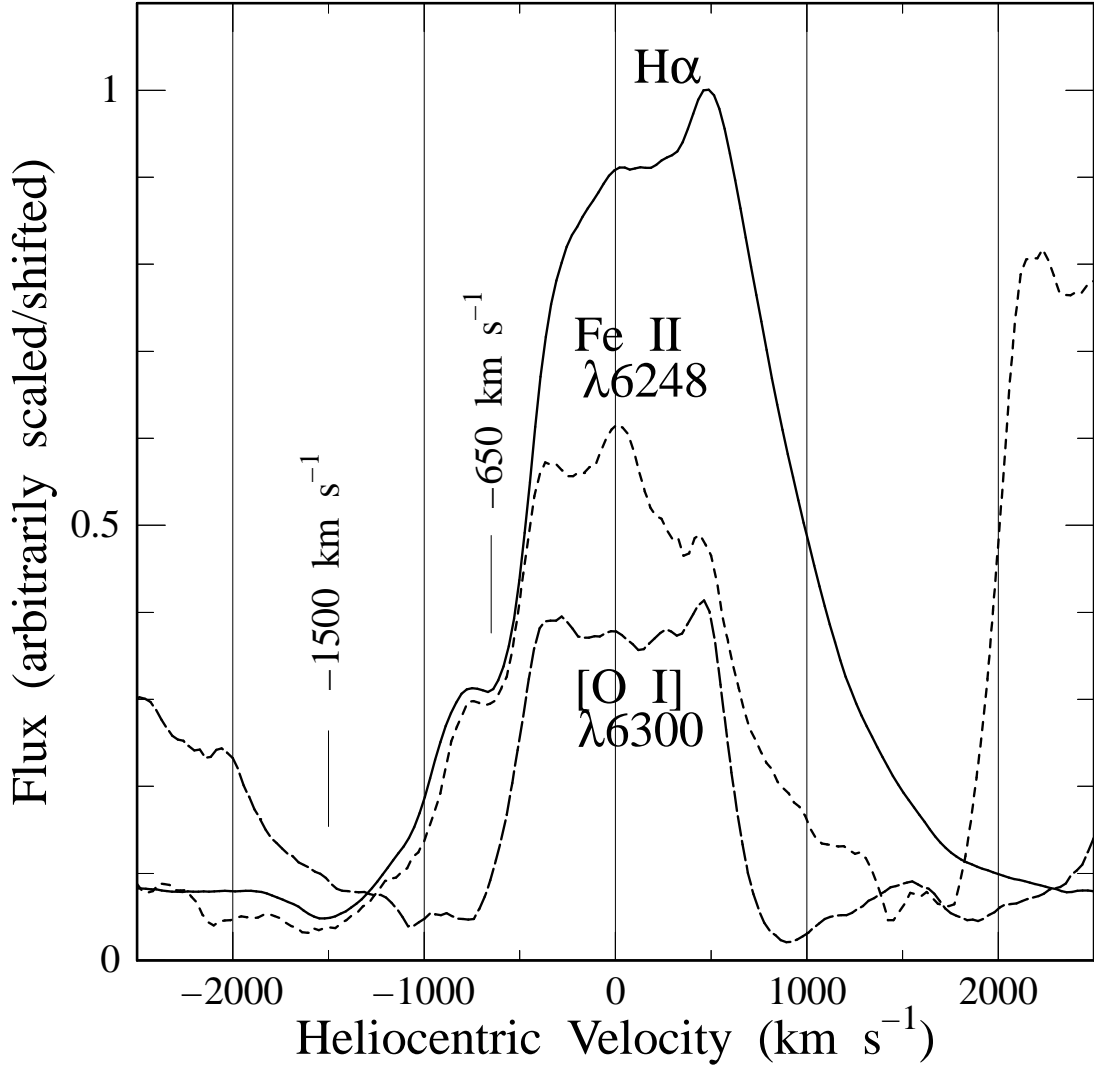


Fig. 4.— Spectral profiles of three prominent emission lines on 36 d. The abscissa is radial velocity simply converted from the observed wavelength. The heliocentric motion of the earth ( $-29.3 \text{ km s}^{-1}$ ) has been corrected. The S/N ratio in each pixel ( $28 \text{ km s}^{-1}$  width) is 80–110 with respect to the neighboring continuum light for each emission line. The velocity resolution, estimated from the FWHM of sky emission lines, is about  $120 \text{ km s}^{-1}$  ( $\simeq 2500$ ), suggesting that the small bumps seen in the emission line profiles are mostly real features. The line widths (FWHM) are  $1450 \text{ km s}^{-1}$ ,  $1300 \text{ km s}^{-1}$  and  $1100 \text{ km s}^{-1}$  for  $\text{H}\alpha$ ,  $\text{Fe II } \lambda 6248$  and  $[\text{O I}] \lambda 6300$ , respectively. It should be noted that  $\text{H}\alpha$  has a distinct red wing.

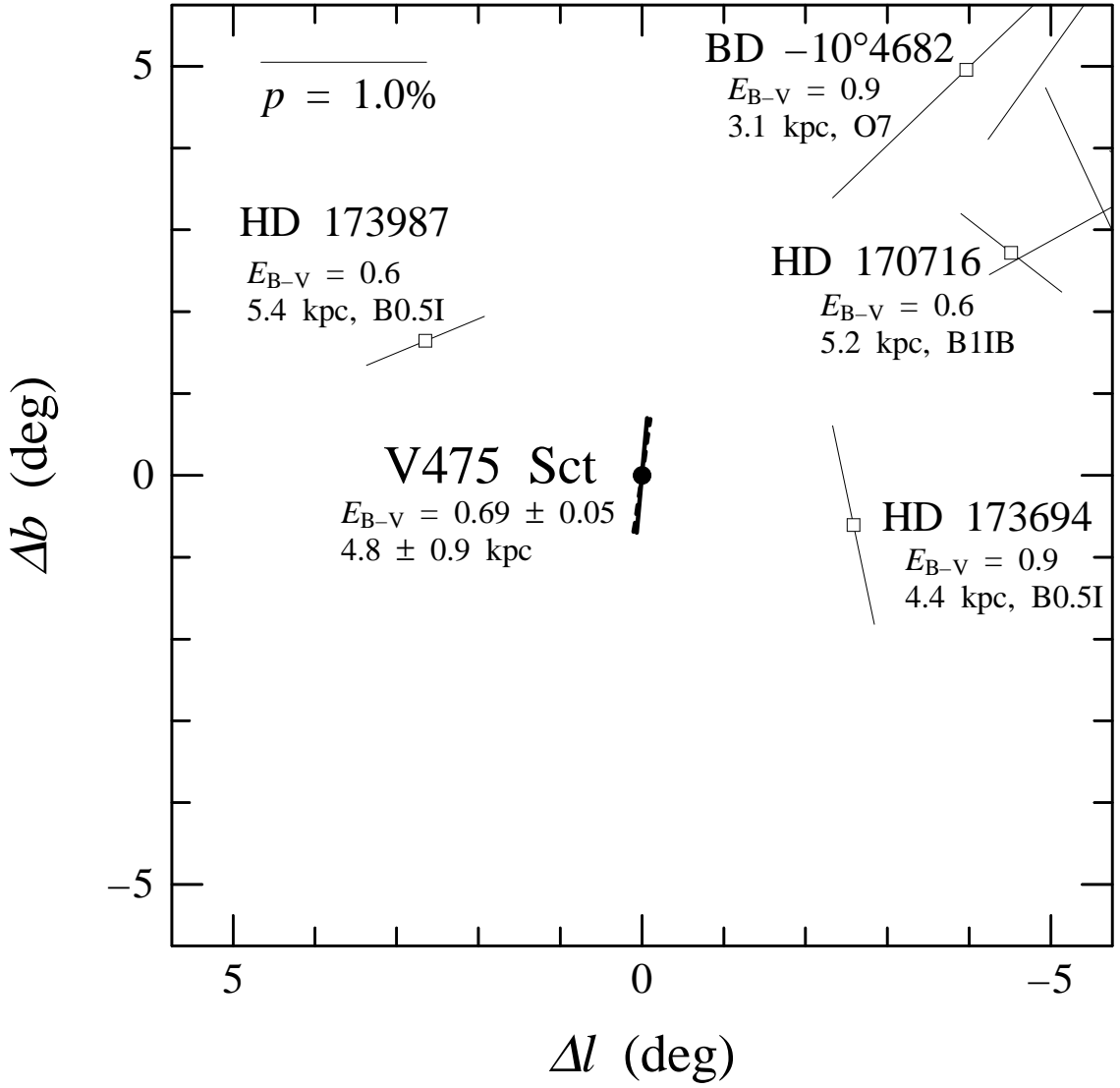


Fig. 5.— Field star polarization map around V475 Sct. Stars at distances of 3–7 kpc are plotted along with star name, color excess, distance and spectral type (Heiles 2000). The magnitude of polarization is proportional to the length of the vectorial bar. The horizontal bar at the top left represents 1.0 % polarization. The ISP components estimated toward V475 Sct are plotted at the origin by solid lines (method 1) and dashed lines (method 3); see the text for details. The distance and color excess of V475 Sct are taken from Chochol et al. (2005). Although the polarization vectors of the field stars have a certain amount of scatter, the derived ISP components seem roughly consistent with the nearest two stars.



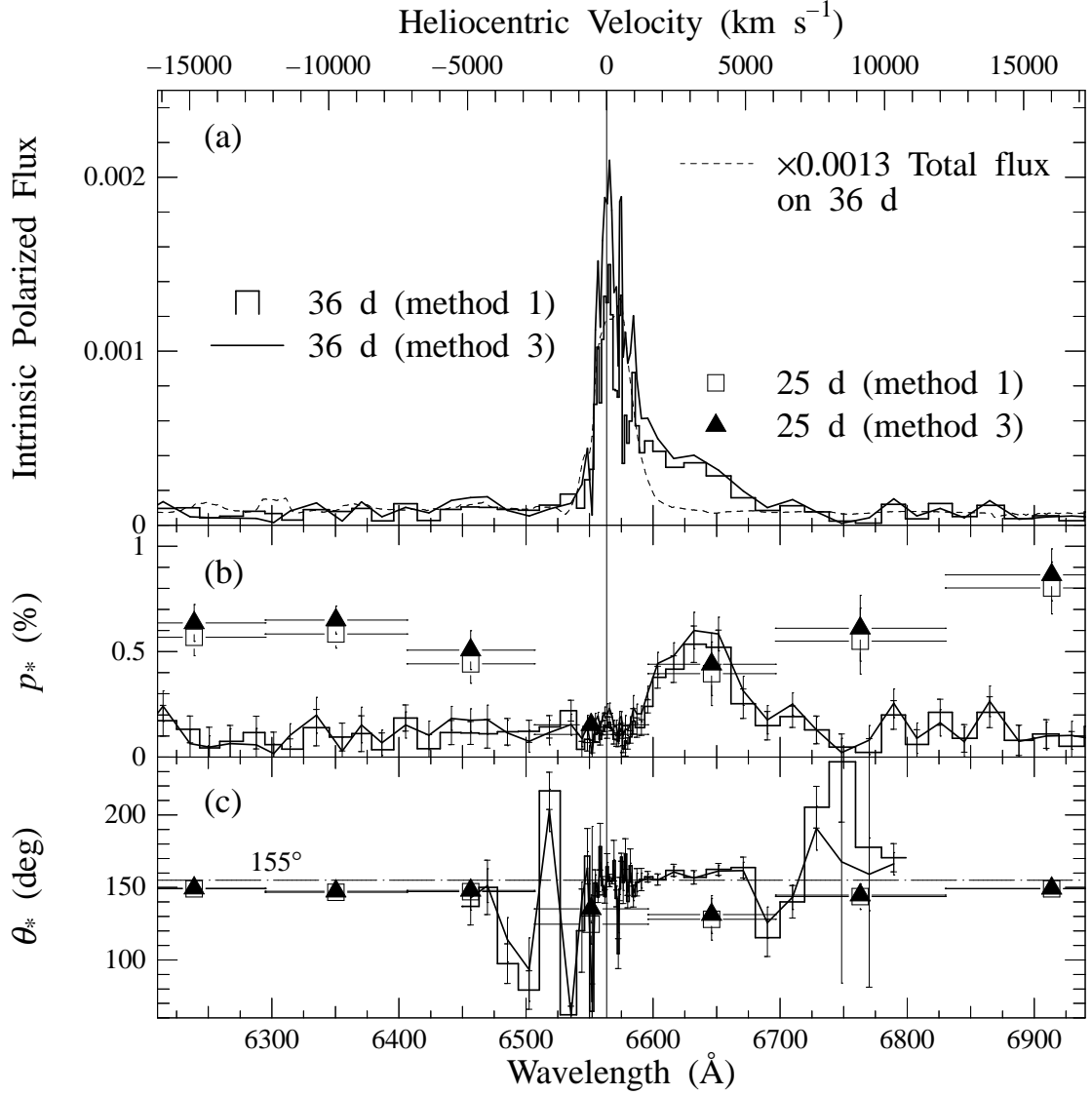


Fig. 6.— Polarization components intrinsic to V475 Sct around H $\alpha$  emission line. We plot (a) polarized flux ( $= p_* \times \text{total flux}$ ) on 36 d, (b) the magnitude of the intrinsic polarization and (c) its PA on both 25 and 36 d. The data are binned in the same manner as in Figures 2 and 3, and the vertical error bars do not include any additional uncertainties from the ISP estimation. In panel (a) the down-scaled total flux is plotted for comparison as a dashed line. In panels (b) and (c) the horizontal error bar of each data point on 25 d indicates the width of the bin. Three bins near the line core seen in Figure 2 have been combined into one to increase the significance. In panel (c) the data on 36 d at wavelength shorter than 6450  $\text{\AA}$  and longer than 6750  $\text{\AA}$  are omitted because of lower signal to noise. The polarized flux has an obvious broad red wing component at  $\theta_* \simeq 155^\circ \pm 15^\circ$ ; the bump in the  $p_*$  spectrum peaks around +3500  $\text{km s}^{-1}$  and extends up to +4900  $\text{km s}^{-1}$ , suggesting the existence of a high-velocity asymmetric wind. The intrinsic polarization of the continuum emission on 25 d has a well fixed PA at  $\theta_* \sim 150^\circ$ , which is similar to that of the wing polarization on 36 d.

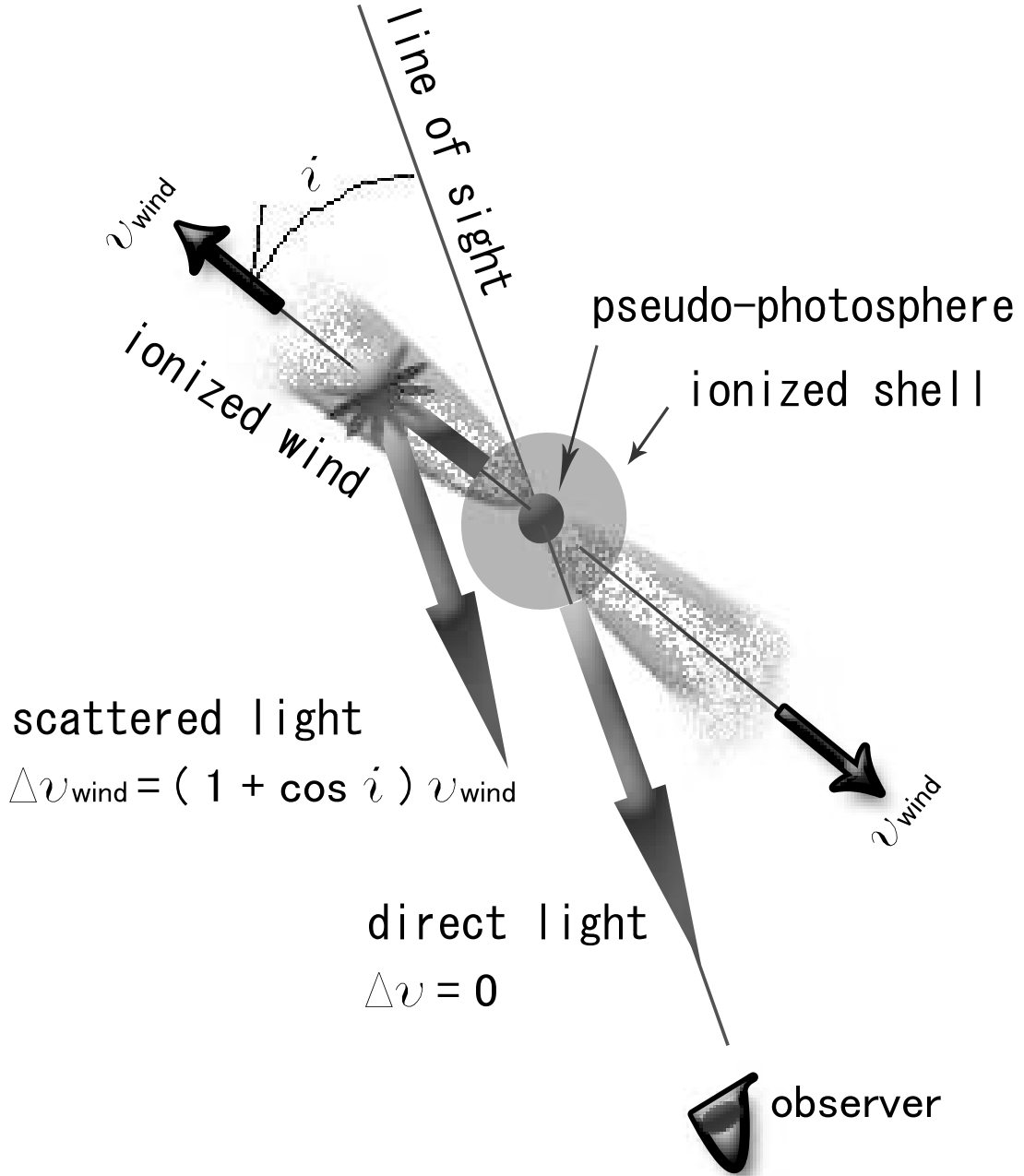


Fig. 7.— Schematic representation of the asymmetric wind model. The nova wind scatters the light from the central region and produces redshifted, polarized light.

Table 2. Polarization component at H $\alpha$  line emission

Epoch	Component	Flux (ADU)	Polarization (%)	Position angle ( $^{\circ}$ )
25 d	Emi+Cont	$7.49 \times 10^5$	$0.585 \pm 0.065$	$115^{\circ}1 \pm 3^{\circ}3$
27 d	Emi+Cont	$9.68 \times 10^5$	$0.632 \pm 0.108$	$103^{\circ}8 \pm 5^{\circ}5$
28 d	Emi+Cont	$1.01 \times 10^6$	$0.581 \pm 0.048$	$108^{\circ}0 \pm 2^{\circ}4$
	Mean		$0.589 \pm 0.037$	$109^{\circ}8 \pm 1^{\circ}8$
25 d	Emi	$6.21 \times 10^5$	$0.533 \pm 0.085$	$110^{\circ}4 \pm 4^{\circ}5$
27 d	Emi	$8.35 \times 10^5$	$0.650 \pm 0.127$	$102^{\circ}6 \pm 6^{\circ}4$
28 d	Emi	$8.16 \times 10^5$	$0.597 \pm 0.063$	$109^{\circ}5 \pm 3^{\circ}0$
	Mean		$0.587 \pm 0.047$	$108^{\circ}7 \pm 2^{\circ}3$

Table 3. Interstellar polarization derived using three methods<sup>a</sup>

Method	$p_{\max}$	$\lambda_{\max}^b$	$\theta_{\text{ISP}}$
1	$0.701 \pm 0.016\%$	$4470 \pm 120\text{\AA}$	$111^{\circ}9 \pm 0^{\circ}3$
2	$0.698 \pm 0.043\%$	$4470 \pm 120\text{\AA}$	$109^{\circ}8 \pm 1^{\circ}8$
3	$0.695 \pm 0.056\%$	$4470 \pm 120\text{\AA}$	$108^{\circ}7 \pm 2^{\circ}3$

<sup>a</sup>See §3.2 and Equations (1) and (2).

<sup>b</sup>Methods 2 and 3 simply use the value derived by method 1.